A Two-α-Helix Extra Domain Mediates the Halophilic Character of a Plant-Type Ferredoxin from Halophilic Archaea[†,‡]

Bianca-Lucia Marg,[§] Kristian Schweimer,[||] Heinrich Sticht,[||,⊥] and Dieter Oesterhelt*[,§]

Max-Planck-Institut für Biochemie, Abteilung Membranbiochemie, Am-Klopferspitz 18a, 82152 Martinsried, Germany, and Lehrstuhl für Biopolymere, Universität Bayreuth, Universitätsstrasse 30, 95440 Bayreuth, Germany

Received July 13, 2004; Revised Manuscript Received October 17, 2004

ABSTRACT: The [2Fe-2S] ferredoxin (HsFdx) of the halophilic archaeon *Halobacterium salinarum* exhibits a high degree of sequence conservation with plant-type ferredoxins except for an insertion of 30 amino acids near its N-terminus which is extremely rich in acidic amino acids. Unfolding studies reveal that HsFdx has an unfolding temperature of ∼85 °C in 4.3 M NaCl, but of only 50 °C in low salinity, revealing its halophilic character. The three-dimensional structure of HsFdx was determined by NMR spectroscopy, resulting in a backbone rmsd of 0.6 Å for the diamagnetic regions of the protein. Whereas the overall structure of HsFdx is very similar to that of the plant-type ferredoxins, two additional α-helices are found in the acidic extra domain. ^{15}N NMR relaxation studies indicate that HsFdx is rigid, and the flexibility of residues is similar throughout the molecule. Monitoring protein denaturation by NMR did not reveal differences between the core fold and the acidic domain, suggesting a cooperative unfolding of both parts of the molecule. A mutant of the HsFdx in which the acidic domain is replaced with a short loop of the nonhalophilic *Anabaena* ferredoxin shows a considerably changed expression pattern. The halophilic wild-type protein is readily expressed in large amounts in *H. salinarum*, but not in *Escherichia coli*, whereas the mutant ferredoxin could only be overexpressed in *E. coli*. The salt concentration was also found to play a critical role for the efficiency of cluster reconstitution: the cluster of HsFdx could be reconstituted only in a solution containing molar concentrations of NaCl, while the reconstitution of the cluster in the mutant protein proceeds efficiently in low salt. These findings suggest that the acidic domain mediates the halophilic character which is reflected in its thermostability, the exclusive expression in *H. salinarum*, and the ability to efficiently reconstitute the iron−sulfur cluster only at high salt concentrations.

Halobacterium salinarum is a halophilic archaeon that is only viable in high salt concentrations (∼2.5−4.3 M NaCl). Halophilic archaea accumulate isotonic concentrations of KCl and NaCl in their cells, and thus, their cell machinery is adapted to function at salt concentrations near saturation (*1*).

Most halophilic enzymes are only active in high salt concentrations, and many halophilic proteins are denatured in low-salt media (*2*). Compared to their mesophilic counterparts, halophilic proteins contain a greater abundance of negatively charged amino acids which increase their stability and solubility in high-salt media. The few known crystal structures of halophilic proteins show that the acidic residues are mainly found on the surface of these proteins (*3*, *4*).

The aim of this work was to identify and analyze additional characteristics of halophilic proteins, accounting for their adaptation to high salt. The *H. salinarum* ferredoxin (HsFdx)[1] was chosen as a model system for these studies because of its peculiar molecular structure.

Ferredoxins are small iron−sulfur proteins present in all organisms which catalyze a large variety of biologically important redox reactions. HsFdx is a [2Fe-2S] ferredoxin of 128 amino acids (*5*) that accounts for 1% of the total soluble protein fraction. It is the electron acceptor for 2-oxoacid oxidoreductases, e.g., the pyruvate:ferredoxin oxidoreductase, and therefore is involved in a central metabolic pathway (*6*).

A comparison of the primary sequence of HsFdx with those of plant-type ferredoxins showed the sequences to be very similar except for an insertion of 30 amino acids near the N-terminus of the halophilic ferredoxin. In the crystal structure of the ferredoxin from the halophilic organism *Haloarcula marismortui*, these 30 amino acids form two

[†] This work was supported by grants from the Boehringer Ingelheim Fonds to B.-L.M. and from the Fonds der Chemischen Industrie to H.S.

[‡] The coordinates have been deposited in the Brookhaven Protein Data Bank (entries 1E0Z and 1E10).

* To whom correspondence should be addressed. Telephone: +49-89-8578 2387. Fax: +49-89-8578 3557. E-mail: oesterhe@biochem.mpg.de.

[§] Max-Planck-Institut für Biochemie.

[||] Universität Bayreuth.

[⊥] Present address: Institut für Biochemie, Emil-Fischer-Zentrum, Friedrich-Alexander-Universität Erlangen-Nürnberg, Fahrstr. 17, 91054 Erlangen, Germany.

[1] Abbreviations: BR, bacteriorhodopsin; CD, circular dichroism; DSC, differential scanning calorimetry; HSQC, heteronuclear single-quantum coherence; HmFdx, *Ha. marismortui* ferredoxin; HsFdx, *H. salinarum* ferredoxin; MDH, malate dehydrogenase; NOESY, nuclear Overhauser effect spectroscopy; NMR, nuclear magnetic resonance; rmsd, root-mean-square deviation.

10.1021/bi0485169 CCC: $30.25
Published on Web 12/10/2004

α-helices (*3*). Almost half (44%) of the residues in this insertion are acidic as compared with 20% for the rest of the protein. Ferredoxins in general are highly negatively charged with a pI of ∼4, and the acidic domain of HsFdx contains an even higher ratio of acidic residues. The high aspartate and glutamate content is characteristic for halophilic proteins, and the acidic insertion probably results in the halophilic behavior of HsFdx.

The high degree of sequence similarity between halophilic ferredoxins and plant-type ferredoxins has been ascribed to lateral gene transfer, and this would require a quick adaptation to high salt concentrations (*7*). This can be achieved faster in evolution by the insertion of a gene fragment than by sequential replacement of single amino acids in the surface. We set out to determine whether this insertion causes indeed the halophilic behavior of HsFdx.

Since halophilism is a phenomenon directly related to solution conditions, we decided to use NMR spectroscopy for our structural studies as it allows the investigation of the influence of different salt concentrations on a protein's structure. NMR spectroscopy also makes it possible to investigate the dynamics of HsFdx and to monitor its denaturation from the iron−sulfur-free form (the HsFdx apoprotein without the Fe_2S_2 cluster) to the unfolded polypeptide chain.

The stability of the halophilic ferredoxin was studied using absorption spectroscopy, CD spectroscopy, and DSC, and refolding of HsFdx as a function of the salt concentration was monitored via reconstitution of its iron−sulfur cluster. To test the functional importance of the acidic insertion in HsFdx, the effect of its replacement with the loop present at the equivalent position in nonhalophilic plant-type ferredoxins was examined. All our results establish the evidence of the acidic extra domain as mediator of the halophilic nature of this ferredoxin.

EXPERIMENTAL PROCEDURES

Bacterial Strains and Vectors. The following strains were used: *H. salinarum* S9 (*8*) [BR^{2+}, HR^+, SRI^+, $SRII^+$, Car^-, Ret^+] and its bacteriorhodopsin deletion strain SNOB (*9*) [BR^-, HR^+, SRI^+, $SRII^+$, Car^-, Rub^-, Ret^+]. *Escherichia coli* strain DH5α (Gibco-BRL) [F^- endA1, hsdR17, supE44, thi-1, recA1, gyrA96, relA1, o80dlacZ M15] was used for cloning and BL21(DE3)RIL as the expression host (*10*) [F^- *ompT hsdS*($r_B^-m_B^-$) dcm^+ Tet^r *gal* λ(DE3) *endA* Hte [*argU ileY leuW* Cam^r]]. Cytoplasmic expression vector pET36b was purchased from Novagen, and pGEX-4T.1 was purchased from Pharmacia Biotech. Vectors pHus-BRFus (*11*) and pBPHM were used for transformation of *H. salinarum*. The Cosmid RI45 (*H. salinarum* strain RI) was used for the PCR of the coding sequence of HsFdx.

Expression in E. coli. The gene encoding HsFdx was amplified from the halobacterial cosmid RI 45 using XbaI and XhoI restriction site-containing oligonucleotide primers for cloning into the pET36b expression vector. The forward primer also contains the *E. coli* ribosomal binding site sequence because cloning using the NdeI restriction site gave no ligation product. The forward primer with restriction sites XbaI and NdeI underlined has the sequence CTAGCTAGTCTAGAAATTTTGTTTAACTTTAAGAAGGAGATATACATATGCCGACGTAGGAATACCTCAACTACAA. The reverse primer (CCGTCCGCTCGAGTCATCAGATGACGCGGTTCTGCAGGTAGTCGAG) contains two stop codons in front of restriction site XhoI (underlined). The XbaI−XhoI fragment from the PCR product was ligated into the XbaI−XhoI-digested pET36b vector. The resulting clones of pET36b-FdxWt were propagated in *E. coli* DH5α cells prior to transformation of *E. coli* BL21(DE3)RIL, which was used as the expression host.

The mutant of HsFdx (Δ-HsFdx) was constructed from pET36b-HsFdx by oligonucleotide-directed mutagenesis in which the two α-helices, α′ and α″, of HsFdx comprising residues 8−36 were replaced with a five-residue loop (EAEGT protein sequence) of *Anabeana* ferredoxin. The following primers were used for replacement: N-terminal primer, 5′-AAC GAA GCC GAG GGC ACG TAC GGC ACG ATG GAG GTC GCG GAG GGC GAG; and C-terminal primer, 5′-GTA CGT GCC CTC GGC TTC GTT GAG GTA TTC TAC CGT CGG CAT ATG. A 3 L culture of (Δ-HsFdx)-pET36b-containing *E. coli* cells was inoculated with a 70 mL overnight culture grown at 37 °C. After 1 h at 25 °C, glucose was added to a concentration of 0.4% (w/v) to prevent leaky expression. Induction of expression was achieved by the addition of isopropyl β-D-thiogalactoside (IPTG) to a final concentration of 1 mM when the OD_{600} of the culture reached 0.5−0.7. The cells were shaken for 3 h at 25 °C before the cells were harvested by centrifugation.

Reconstitution and Purification of Δ*-HsFdx. E. coli* BL21(DE3)RIL cell pellets, transformed with pET36b-(Δ-HsFdx), were resuspended in 25 mM Tris-HCl buffer (pH 8.5) containing DNAse and a protease inhibitor mix without EDTA (supplied from Boehringer). The cells were disrupted using a French press, and the homogenate was centrifuged for 10 min at 20000*g* before urea and DTT were added to the supernatant to final concentrations of 8 M and 100 mM, respectively. To reconstitute the iron−sulfur cluster into the expressed apo-Δ-HsFdx, this solution was gassed with nitrogen for 0.5 h (*12*), and $FeSO_4$ and Na_2S were both added to a final concentration of 10 μM. After incubation for 10 min under nitrogen, 7 volumes of 25 mM Tris-HCl (pH 8.5) that had been gassed with nitrogen prior to use was added. Then the same volume of oxygen containing Tris buffer was added. To test the influence of the NaCl concentration on the reconstitution of the iron−sulfer cluster into apo-Δ-HsFdx as well as the stability of Δ-HsFdx in solutions having different salt concentrations, reconstitution of the mutant ferredoxin was performed in the crude cytosolic fraction as described above except that Tris-HCl (pH 8.5) buffers having different NaCl concentrations were used.

The solution resulting from the above reconstitution treatment using NaCl-free Tris-HCl (pH 8.5) buffer was concentrated on DEAE-Sephacel which had been equilibrated with 25 mM Tris-HCl (pH 8.5) and 0.1 M NaCl. The DEAE was washed with the equilibration buffer, and Δ-HsFdx eluted as a brown band with 25 mM Tris-HCl (pH 8.5) and 1 M NaCl. The eluate was diluted to 0.2 M NaCl, buffered with 10 mM Na_2HPO_4/NaH_2PO_4, and applied on a Q-Sepharose fast flow column, and Δ-HsFdx eluted at a concentration of ∼0.33 M NaCl and was further purified on a hydroxyapatite column [Na_2HPO_4/NaH_2PO_4 (pH 7.5) from 10 to 50 mM, with 0.2 M NaCl] and finally gel filtered (Superose-12 from Pharmacia). The GST fusion proteins

(Table 3) were purified according to the protocol from Pharmacia Biotech.

Expression of Ferredoxins in H. salinarum and Purification. The transformation of the halobacterial cells was performed according to a previously published protocol (*13*). For the selection of transformants, mevinolin was used. Cell lysis was performed by dialysis against water overnight at 4 °C or via sonification in a 4 M NaCl solution. The His-tagged protein was purified on a Ni−NTA column. The cell extract was prepared by sonification of the *H. salinarum* cells in 4.3 M NaCl. The BR fusion protein was prepared according to the standard protocol for the isolation of purple membranes, including the dialysis of the cells against water for cell disruption (*14*). The purified fusion protein was cleaved with factor Xa.

Apoprotein Preparation and Reconstitution of HsFdx. Trichloroacetic acid (10%) was added at 4 °C to 1 mL HsFdx (50 μM) solution to a final concentration of 0.4% which is accompanied by a gradual discoloring of the solution. The mixture was incubated while being agitated for 15 min at 4 °C. After centrifugation at 14 000 rpm for 10 min, the supernatant was discarded and the pellet redissolved in 400 μL of a solution of 100 mM Tris (pH 9.0), 100 mM DTT, and 8 M urea. After incubation under nitrogen for 40 min, 20 μL of 100 mM Na_2S and 100 mM $FeSO_4$ was added. After 30 min at room temperature, the solution was diluted to 6 mL with a solution of 100 mM Tris (pH 8.5) and *x* M NaCl (*x* is variable) and afterward dialyzed for 2 h against a solution of 10 mM Tris-HCl (pH 8.0) and *x* M NaCl. The dialysis buffer was exchanged for a solution of 10 mM Na_2HPO_4/NaH_2PO_4 buffer (pH 7.3) and *x* M NaCl for final dialysis overnight.

UV−Vis and CD Spectroscopy and DSC. The absorption spectra of the HsFdx apoprotein treated as described above with different NaCl concentrations (0 mM, 0.15 mM, 0.43 mM, 2.0 M, and 4.3 M) were acquired on an Aminco DW-2a UV−vis spectrophotometer (see Table 4). For the CD spectra, a Jasco J-715 spectropolarimeter was used, and the DSC spectra were recorded on a Microcal VPDSC instrument.

Sample Preparation for NMR Measurements. Since NMR spectroscopy allows the investigation of structures in atomic detail in solution, it can be used to study the role of different parts of HsFdx in halophilic adaptation. For the acquisition of the NMR spectra, HsFdx has to retain its tertiary structure for ∼2 weeks, and the salt concentration has to be sufficiently low to avoid a loss of sensitivity due to radio frequency absorption. On the basis of the results of the experiments described above, suitable solution conditions could be identified (Figure 1, bottom). HsFdx samples had an A_{420}/A_{280} ratio of >0.3 in 450 mM NaCl (pH 6.5) (50 mM sodium phosphate buffer) at 15 °C after the end of the NMR experiment.

NMR Spectroscopy. All NMR spectra were recorded on a Bruker DRX 600 NMR spectrometer with pulsed field gradient capabilities at 15 °C on samples containing 0.8−1.0 mM protein, 50 mM potassium phosphate (pH 6.5), and 450 mM sodium chloride, in a 9:1 H_2O/D_2O mixture. In addition to the experiments described previously (*15*), the following experiments were conducted to collect NOE data: three-dimensional (3D) ^{15}N NOESY-HSQC (mixing time of 120 ms) (*16*), 3D ^{13}C NOESY-HSQC (mixing time of 120 ms) (*17*), and 3D ^{15}N HMQC-NOESY-HSQC (mixing time of 150 ms) (*18*). In the amide-detected experiments, a binomial 3-9-19 WATERGATE sequence (*19*) with water flip-back was employed for water suppression, and in the ^{13}C-edited NOESY experiments, gradient coherence selection (*20*) was employed for water suppression. Quadrature detection in the indirect dimensions was achieved by the States−TPPI method (*21*).

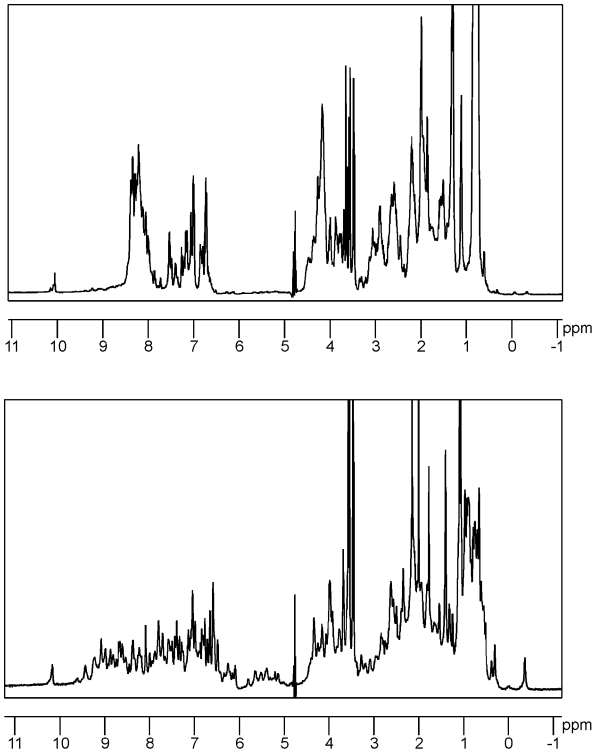

FIGURE 1: 1D ^{1}H spectra of a HsFdx solution [∼1 mM HsFdx in 10 mM phosphate buffer (pH 6.5) containing 450 mM NaCl] with different A_{420}/A_{280} ratios: (top) 1D ^{1}H NMR spectrum of HsFdx for which $A_{420}/A_{280} = 0.25$ and (bottom) 1D ^{1}H NMR spectrum of HsFdx for which $A_{420}/A_{280} = 0.33$.

Slowly exchanging amide protons were identified from a series of ^{15}N−^{1}H HSQC spectra that were recorded after the lyophilized protein had been dissolved in D_2O (99.996%). The $\{^1H\}^{15}N$ NOE experiments were carried out using the pulse sequences of Dayie and Wagner (*22*). The relaxation delay was 7 s, and the proton saturation was performed with 120° high-power pulses with an interpulse delay of 5 ms for the final 3 s of the relaxation delay of the saturation experiment. Saturated and unsaturated spectra were measured in an interleaved mode to minimize problems of sample stability. Experiments were repeated twice to obtain an estimation of the error in the $\{^1H\}^{15}N$ NOE values. Residues exhibiting a standard deviation for the measured $\{^1H\}^{15}N$ NOE of >0.1 between the two experiments or which suffered from a poor signal-to-noise ratio due to their proximity to the metal center (<10 Å) were excluded from the calculation. The NMR data were processed using software written in-house and analyzed with NMRView (*23*) and NDEE (SpinUp Inc., Dortmund, Germany).

Structure Calculation and Analysis. On the basis of the assignment of the ^{1}H, ^{13}C, and ^{15}N resonances of HsFdx (*15*), a total of 1258 NOE distance restraints could be derived from the two- and three-dimensional NOESY spectra in an iterative procedure (Table 1). NOE cross-peaks were manu-

Table 1: Unfolding Transition Temperatures (T_m) of HsFdx (~220 μM) in 10 mM Na_2HPO_4/NaH_2PO_4 Buffer (pH 7.3) Containing Different Concentrations of NaCl[a]

salt concentration	T_m (DSC) (°C)	T_m (CD) (°C)
100 mM NaCl	49.5	49
430 mM NaCl	56	56
4.3 M NaCl	85	–

[a] The measurements were performed at a wavelength of 222 nm using a temperature scan rate of 1 °C/min.

ally classified as strong, medium, or weak according to their intensities and converted into distance restraints of less than 2.7, 3.5, or 5.0 Å, respectively. A total of 56 residues exhibited $^3J_{HNH\alpha}$ scalar coupling constants of either <6.0 or >8.0 Hz and were therefore restrained to adopt backbone torsion angles between −80° and −40° or between −160° and −80°, respectively. A hydrogen bond was assumed if the acceptor of a slowly exchanging amide proton could be identified unambiguously from the results of initial structure calculations. For each of the 46 hydrogen bonds, the distance between the amide proton and the acceptor was restrained to less than 2.3 Å and the distance between the amide nitrogen and the acceptor to less than 3.3 Å.

The highly invariant geometry of the [2Fe-2S] cluster was maintained by 12 dihedral angle restraints for the cluster and for the side chains of the ligating cysteines that were deduced from the HmFdx crystal structure (*3*). These restraints served as an input for the structure calculation with X-PLOR, version 3.851 (*24*), using a three-stage simulated annealing protocol (*25*) with floating assignment of prochiral groups (*26*). For conformational space sampling, 120 ps with a time step of 2 fs was simulated at a temperature of 2000 K, followed by slow cooling for 90 ps to 1000 K and cooling for 45 ps to 100 K, both with a time step of 1 fs.

In a second simulation, structural information for residues 60−72, 87, and 100−106 which are experimentally underdetermined from NMR spectroscopy due to the spatial proximity to the paramagnetic iron−sulfur cluster was deduced from the crystal structure of HmFdx. Pairwise interresidue distance restraints were derived between the Cα atom and one side chain heavy atom of each of these residues, and their backbone ϕ and ψ angles were restrained to be within an interval of ±10°. No additional distance restraints to amino acids from other parts of the sequence were included in the calculation to prevent interference with the NMR experimental data. Otherwise, the structure calculation was identical to that described above.

Of the 60 structures resulting from the final round of each structure calculation, those 20 structures that exhibited the lowest energy and the fewest violations of the experimental data were selected for further characterization. The geometry of the structures, structural parameters, and elements of secondary structure were analyzed using DSSP (*27*), PROCHECK (*28*), and DALI (*29*). For the graphical presentation of the structures, SYBYL 6.5 (Tripos), GRASP (*30*), MOLSCRIPT (*31*), and Raster3D (*32*) were used. The coordinates for the family of structures calculated with and without additional restraints for the cluster vicinity have been deposited in the Protein Data Bank as entries 1E0Z and 1E10, respectively.

RESULTS AND DISCUSSION

Protein Preparation. HsFdx was first isolated at a low salt concentration according to the protocol of Oesterhelt and Kerscher (*33*). The purified protein with an A_{420}/A_{280} ratio of 0.2 exhibited a single band in SDS−PAGE. As judged from the one-dimensional (1D) NMR spectrum of the HsFdx, large quantities of the unfolded protein are present (Figure 1, top). A purification for the homologous ferredoxin of *Ha. marismortui* (HmFdx) has been established by Werber and Mevarech (*34*), which does not require exposure of the halophilic protein to low salt concentrations, as all the steps are carried out at molar concentrations of NaCl or $(NH_4)_2SO_4$ which results in an A_{420}/A_{280} ratio of 0.33 for the purified HmFdx. Two chromatographic steps from the HmFdx purification protocol were applied to HsFdx, and samples with A_{420}/A_{280} ratios of ≥0.3 were obtained. The 1D spectra of theses samples indicate that the protein exhibits intact tertiary structure (Figure 1, bottom). All further experiments were performed using HsFdx preparations with an A_{420}/A_{280} ratio of ≥0.3 to ensure that the protein is properly folded.

Stability Measurements: T_m Values of HsFdx as a Function of the Salt Concentration. The effect of varying the salt concentration of the solution on the T_m values of HsFdx has been determined by differential scanning calorimetry (DSC) and circular dichroism (CD) spectroscopy at a wavelength of 222 nm using a scan rate of 1 °C/min. Both methods gave similar results, and it was seen that increasing the salt concentration leads to a considerable enhancement of the protein's stability (Table 1 and Figure 2b).

Temperature Dependence of the Denaturation of HsFdx. The change in absorption of HsFdx at 420 nm with an increase in temperature was studied by absorption spectroscopy. The lower the salt concentration, the lower the temperature at which irreversible denaturation of the ferredoxin occurs, as judged by the decrease in absorption at 420 nm accompanying the destruction of the [2Fe-2S] cluster (Figure 2a). Furthermore, an influence of the heating rate on the denaturation curve was noticed for higher salt concentrations: in 4.3 M NaCl, the curve is shifted to higher temperatures when the heating rate increases, meaning that higher temperatures are reached before the same degree of denaturation is obtained. This indicates that the rate of thermal denaturation of HsFdx is in the time range of the heating rate (time scale of minutes). Such a slow denaturation may be the result of partially denatured, high-energy intermediate states of HsFdx, which are passed during the denaturation process.

From the T_m values (Table 1) and the results of the absorption measurements (Figure 2a), we conclude that HsFdx is a halophilic protein: its high thermostability in high-salt media is essential under physiological conditions because halobacteria are preferentially found in warmer regions where highly concentrated salty water occurs. Work to this point allows us to compare the halophilic nature of HsFdx with other haloarchaeal proteins but does not yet identify the structural elements responsible for it. This was achieved in the experiments described below.

Comparison of the Stability of HsFdx to the Stabilities of Other Halophilic Proteins. It has been demonstrated previously with absorption and fluorescence measurements as well as by CD spectroscopy at room temperature that the protein

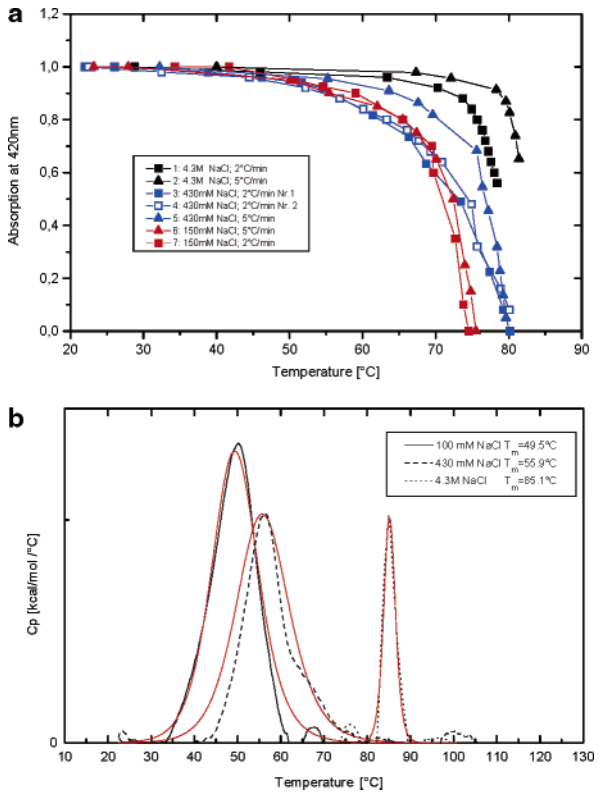

FIGURE 2: (a) Absorption at 420 nm of HsFdx solutions containing different NaCl concentrations in correlation to the temperature variation measured using different heating rates. (b) DSC spectra of HsFdx in solutions having different salt concentrations (100 mM, 430 mM, and 4.3 M NaCl). The spectra were acquired using a temperature scan rate of 1 °C/min. The measured curves are depicted in black and the calculated ones in red.

tolerates NaCl concentrations down to 0.5 M NaCl (*35*), but its stability increases with higher salt concentrations. Below 0.5 M NaCl, a decrease in absorption, fluorescence intensities, and overall ellipticity over time was observed.

HsFdx denatures (unfolds) very slowly at low salt concentrations compared to other halophilic proteins. In 50 mM NaCl, it takes ~48 h at room temperature until the absorption intensity at 420 nm reaches half the starting value. In contrast, the unfolding of *Ha. marismortui* malate dehydrogenase (MDH) at low salt concentrations is finished within several minutes (*36*). However, if the cofactor NADH is added to the HmMDH solution before it is diluted to low salt concentrations, the half-life of the halophilic protein is considerably increased and the denaturation takes more than 24 h (*36*). A stabilizing effect similar to that of NADH on HmMDH can be ascribed to the iron−sulfur cluster in HsFdx.

At high salt concentrations (4.3 M NaCl), HsFdx shows thermal stability comparable to that of other halophilic proteins: at 67 °C, the half-life of HsFdx is ~48 h. In 4.3 M NaCl, it is not possible to denature HsFdx by the addition of urea. At low salt concentrations on the other hand, a slight displacement of the absorption maxima in the visible range is observed and has been interpreted as a change in structure at low ionic strength by Sonawat et al. (*37*). The change in the absorption maximum could be further increased by the addition of urea (data not shown). This indicates that a partly denatured form of holo-HsFdx containing the [2Fe-2S] cluster exists at low salt concentrations, confirming the NMR results (Figure 1).

Table 2: Summary of Structure Calculation

Experimental Restraints for the Final Structure Calculation	
total no. of NOEs	1258
intraresidual ($\|i-j\|=0$)	393
sequential ($\|i-j\|=1$)	336
medium-range ($\|i-j\|\leq 5$)	195
long-range ($\|i-j\|>5$)	334
no. of $^3J(H^N,H^\alpha)$ dihedral restaints	56
no. of hydrogen bonds[a]	92

Molecular Dynamics Statistics	with additional cluster restraints	without additional cluster restraints
average energy (kcal/mol)		
E_{tot}	24.21 ± 1.96	17.70 ± 1.57
E_{bond}	1.35 ± 0.08	1.15 ± 0.07
E_{angles}	10.91 ± 0.90	9.00 ± 0.55
$E_{improper}$	1.64 ± 0.17	1.40 ± 0.08
E_{repel}	5.61 ± 1.24	3.04 ± 1.02
E_{NOE}	4.60 ± 1.21	3.12 ± 0.84
E_{cdih}	0.10 ± 0.01	0.01 ± 0.007
rmsd from ideal distances (Å)		
NOE	0.006 ± 0.0008	0.006 ± 0.0008
bonds	0.001 ± 0.00002	0.001 ± 0.00002
rmsd from ideal angles (deg)		
bond angles	0.14 ± 0.006	0.13 ± 0.004
improper angles	0.10 ± 0.003	0.09 ± 0.003

Atomic rms Differences (Å)	with additional cluster restraints	without additional cluster restraints
overall (residues 1−128)[b]	0.82/1.31	nd[d]
"diamagnetic region"[b]	0.66/1.18	0.81/1.33
regular secondary structure[b]	0.50/0.95	0.60/1.05
HsFdx vs HmFdx[c]	1.3 (122)	
HsFdx vs *Anabaena* Fdx[c]	1.8 (96)	
HsFdx vs *E. arvense* Fdx[c]	1.6 (94)	

[a] Two restraints were used for each hydrogen bond (see Experimental Procedures). [b] Calculated for the final set of 20 structures (backbone atoms/all heavy atoms); diamagnetic region, residues 1−59, 73−86, 88−99, and 107−122; regular secondary structure, residues 2−14, 23−30, 37−43, 48−55, 72−75, 79−83, 90−96, 98−100, 104−106, 110−115. [c] Calculated from a DALI (*29*) pairwise comparison of the HsFdx average structure (residues 1−122) with the crystal structures of *Ha. marismortui* Fdx (*3*), *Anabaena* 7120 Fdx (*49*), and *E. arvense* Fdx (*50*). The number of structurally equivalent residues is given in parentheses. [d] Not determined.

Strategy for Structure Determination. Analysis of the NMR spectra of HsFdx yielded a total of 1406 experimental restraints for the structure calculation (Table 2). Because of the good dispersion of the amide proton resonances (*15*), most NOE distance restraints were obtained from the ^{15}N NOESY-HSQC spectrum. The ^{13}C NOESY-HSQC spectrum suffered from an unsatisfactory signal-to-noise ratio due to fast paramagnetic relaxation and the low protein solubility (0.8−1.0 mM), which was worsened by the presence of some degradation products in the sample. As a consequence, only a few distance restraints were derived from this spectrum. The temperature (15 °C) and salt concentration (0.45 M) that were used represent a compromise to allow a sufficient protein solubility and stability for the time of the NMR measurements. Significant amounts of degradation products (and/or apoprotein) impairing the evaluation of the NMR data were apparent after 1−2 weeks. Additional ^{15}N HSQC

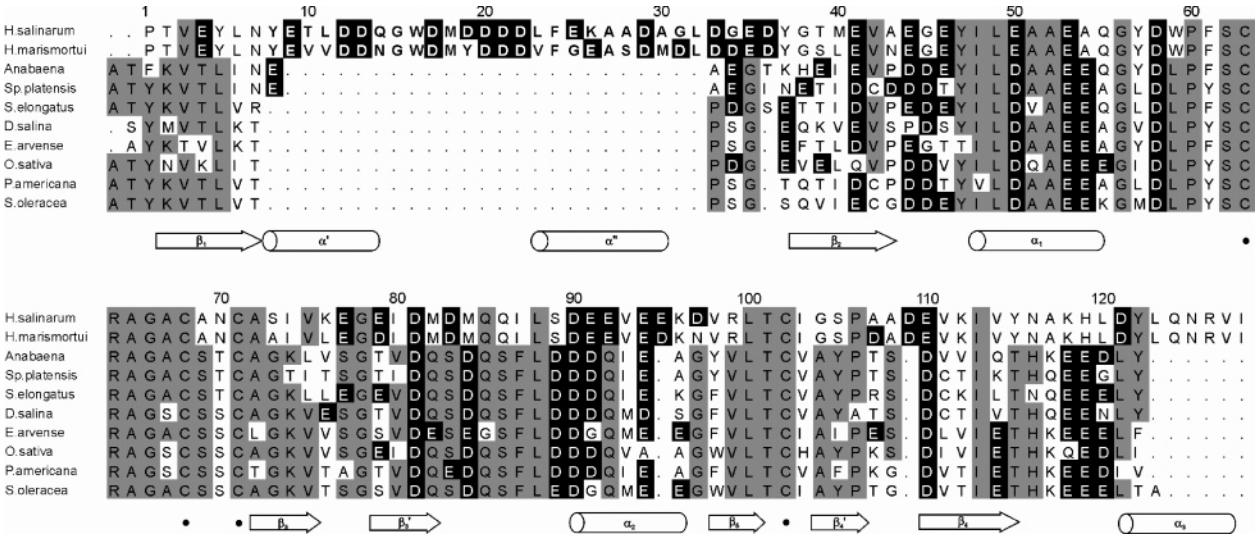

FIGURE 3: Sequence alignment of halobacterial and plant-type ferredoxins. Sequence alignment of [2Fe-2S] ferredoxins from two halobacteria (*H. salinarum* and *Ha. marismortui*), blue-green algae (*Anabaena* 7120, *Spirulina platensis*, and *Synechococcus elongatus*), a green alga (*Dunaliella salina*), and plants (*E. arvense*, *Oryza sativa*, *Phytolacca americana*, and *Spinacia oleracea*). The *H. salinarum* numbering scheme is given at the top. The four cluster ligating cysteines are denoted with black circles (•). Acidic residues are highlighted with black boxes, and residues occurring with a frequency of >50% are highlighted with gray boxes. Elements of secondary structure present in the *H. salinarum* structure are given below the alignment. The extra domain, which is not present in plant-type ferredoxins, is marked with bold letters. The alignment was generated by combining sequence and structure information using ClustalW (*64*) and DALI (*29*) and for graphical representation Alscript (*65*).

spectra measured at a salt concentration of 1.5 M were virtually identical to those at 0.45 M, confirming that the structure remains unaltered at salt concentrations as low as 0.45 M. Furthermore, this finding shows that the decreased protein stability observed at lower salt concentrations does not reflect structural differences, but is rather due to a lowered energy barrier of unfolding.

Additional factors that influence the quality of the experimental data and thus the quality of the calculated structures are paramagnetic effects arising from the iron−sulfur cluster. These paramagnetic effects generally result in the absence of detectable NMR signals for the protons in the vicinity of the cluster (*38*, *39*). Therefore, to allow a comparison of the overall HsFdx structure to its homologues, the conformation of paramagnetically affected residues 60−72, 87, and 100−106 was modeled on the basis of the geometry observed for these residues in the crystal structure of HmFdx (*3*). Such a strategy for modeling the cluster vicinity has already been used previously to compensate for the lack of NMR distance restraints (*40*−*42*) and appears to be justified for HsFdx, particularly because it has the same sequence as HmFdx in this part of the molecule (Figure 3). Alternative strategies for obtaining structural information about the cluster vicinity in [2Fe-2S] ferredoxins such as the substitution of the paramagnetic iron with diamagnetic gallium (*43*−*45*) or the application of special NMR techniques that are suitable for paramagnetic systems (*42*, *46*, *47*) were not feasible for HsFdx. A substitution of iron with gallium in the HsFdx reconstitution failed (data not shown), and the application of "paramagnetic" NMR spectroscopy which generally suffers from a poor signal-to-noise ratio was impeded by the low sample concentration resulting from poor protein solubility.

Analysis of the HsFdx Structure. Both sets of structures calculated with and without additional restraints for the cluster vicinity exhibit quite similar rmsd values for the diamagnetic part of the molecule (Table 2), proving that the NMR data alone were sufficient to establish the correct folding topology. Thus, to our knowledge, the HsFdx structure represents the first structure of a halophilic protein that was determined in solution. The observation that the rmsd values are generally slightly lower in the structures calculated with additional restraints for the cluster vicinity can be explained by the fact that fixation of the connecting loops also has some effect on defining the conformation of the adjacent residues. Furthermore, the backbone rmsd between the minimized average structures from both calculations is 0.43 Å, showing that the inclusion of additional cluster restraints does not significantly distort the remaining parts of the molecule. For these reasons, all subsequent analyses were performed for the family of structures calculated with the additional cluster restraints.

Analysis of HsFdx with PROCHECK (*28*) revealed seven strands of β-sheet and five α-helices as major elements of secondary structure: β_1 (2−7), β_2 (37−43), β_3 (72−75), β_3' (79−83), β_5 (98−100), β_4' (104−106), β_4 (110−115), α' (8−14), α'' (23−30), α_1 (48−55), α_2 (90−96), and α_3 (121−126) (Figures 3 and 4b). The overall orientation of this latter helix α_3 toward the rest of the molecule is not well-defined in the NMR set of structures as an indirect effect from the paramagnetic metal center (Figure 4a). In the crystal structure of the homologous HmFdx (*3*), the C-terminal end of this helix packs against a cluster-ligating loop (residues 60−72) for which resonances could not be assigned in HsFdx. Therefore, no long-range NOEs between residues 67−72 and residues 127 and 128 could be observed that would allow a better definition of the orientation of helix α_3.

Strands β_1−β_5 form a five-stranded mixed β-sheet, in which all strands with the exception of parallel strands β_1 and β_4 are aligned in an antiparallel fashion (Figure 4b). The topology of this β-sheet is identical to that observed for HmFdx and highly similar to that of plant-type ferredoxins which sometimes lack strand β_5. Additional elements of secondary structure, including a short antiparallel β-sheet

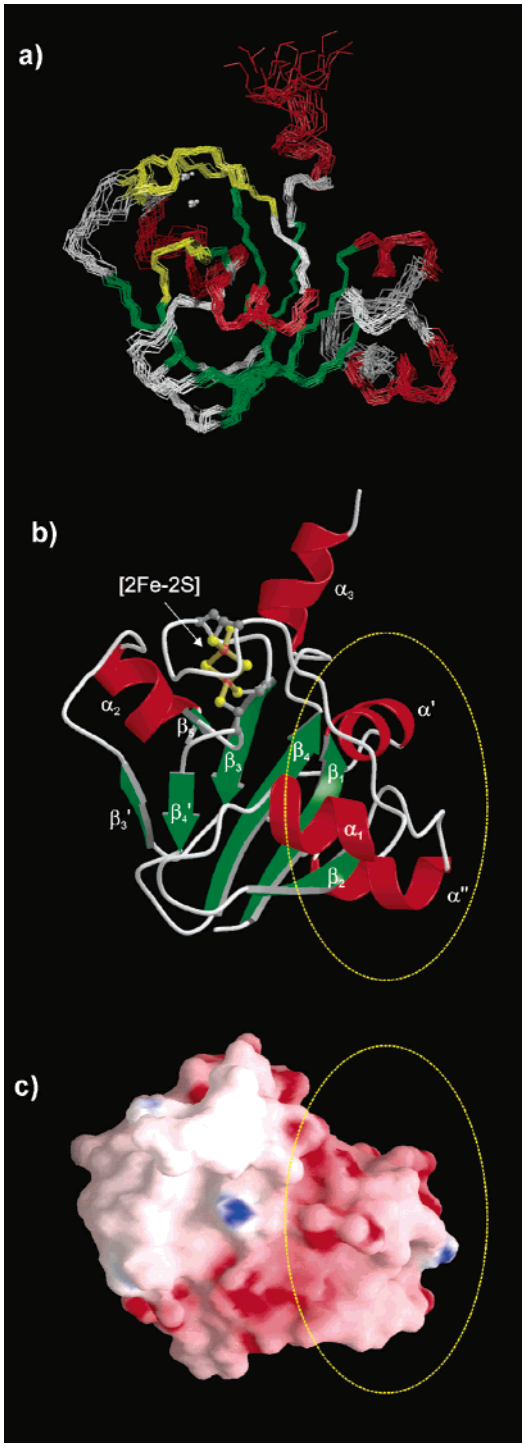

FIGURE 4: (a) Backbone overlay of a family of 15 *H. salinarum* ferredoxin structures. β-Strands are colored green and helices red. The cluster region that was modeled on the basis of the homology to the ferredoxin from *Ha. marismortui* is colored yellow. The iron atoms that give rise to the paramagnetic effects are represented as white balls. (b) Schematic presentation of the *H. salinarum* ferredoxin indicating the elements of secondary structure. The iron−sulfur cluster and the ligating cysteines are shown in ball-and-stick representation. (c) Electrostatic potential at the HsFdx protein surface. Positive and negative charges are colored blue and red, respectively. The magnitude of the charges is indicated by the intensity of the color. The extra domain that carries a large excess of negative charges is marked with a yellow ellipse. This view differs from Figure 4b by a rotation of approximately 90° around the horizontal axis, placing helix α_3 on top of the presentation. This figure was prepared with Sybyl 6.5 (Tripos), Molscript (*31*), Raster3D (*32*), and Grasp (*30*).

(residues 79−83 and 104−106) and helices α_1 and α_2, were also found previously in homologous [2Fe-2S] ferredoxins (*48*).

On the level of tertiary structure, HsFdx can be overlaid with the structures of *Anabaena* 7120 (*49*) and *Equisetum arvense* (*50*) ferredoxin with Cα rmsds of 1.8 and 1.6 Å for a set of 96 and 94 equivalent residues, respectively (Table 2). Therefore, the core fold (residues 1−5 and 39−128) of HsFdx can be considered structurally equivalent to that of the plant-type ferredoxins (Figures 3 and 5). DALI analysis allowed the unambiguous identification of the two additional amino acids present in the HsFdx core fold (Figure 3) which have no structural equivalent in plant-type ferredoxins. Interestingly, both one-residue insertions (positions 95 and 109) are occupied by negatively charged residues. These residues may also play a role in halophilic adaptation in addition to the acidic domain, as they are located on the surface and this is the location of acidic amino acid side chains for long-term halophilic adaptation.

This N-terminal acidic domain (residues 7−36), which is unique to halophilic ferredoxins, is inserted between strands β_1 and β_2 of the core fold (residues 1−6 and 37−128), replacing a turn or loop that connects these two strands in the plant-type ferredoxins (Figure 3). It contains a large number of acidic residues (Figures 3 and 4c), providing numerous surface carboxylates with strong water binding ability. These residues were shown to play a role in stabilizing a halophilic malate dehydrogenase at high salt concentrations (*51*, *52*) and preventing self-aggregation (*3*).

This extra domain is >15 Å from the cluster and is therefore not affected by paramagnetic effects, making the NMR structure determination straightforward. It contains two helices, α′ (residues 8−14) and α″ (residues 23−30), connected by a loop which adopts an overall geometry similar to that of the corresponding structural element in HmFdx (Figure 5). The only notable difference from the HmFdx crystal structure is the orientation of W16 within the acidic domain. The ring of this residue forms numerous hydrophobic contacts with L6, V11, and V23 in the HmFdx crystal structure, while the absence of NOEs for the ring of W16 in the NMR spectra of HsFdx suggests that this residue does not form extensive hydrophobic contacts in solution. The lack of NOEs, however, might also result from increased flexibility in solution, consistent with the observation that the extra domain was not well-defined in the first crystallographic studies of HmFdx (*2*).

Apart from this local structural difference, the HsFdx and HmFdx structures are highly similar (1.3 Å Cα rmsd for residues 1−122), indicating that the different methods used for structure determination and the different experimental conditions (HmFdx, crystallized from solutions of 3.8 M sodium and potassium phosphate; HsFdx, NMR at an ionic strength of 0.5 M) did not have a substantial impact on the structure obtained. It remains to be shown that NMR spectroscopy and X-ray crystallography produce similar results for the structure determination of other halophilic proteins. In addition to these structural comparisons, the application of NMR spectroscopy in this study offered the opportunity to perform subsequent experiments investigating the dynamics and stability of HsFdx at atomic resolution.

Dynamics of HsFdx. $\{^1H\}^{15}N$ NOE experiments were performed to investigate the backbone flexibility of HsFdx

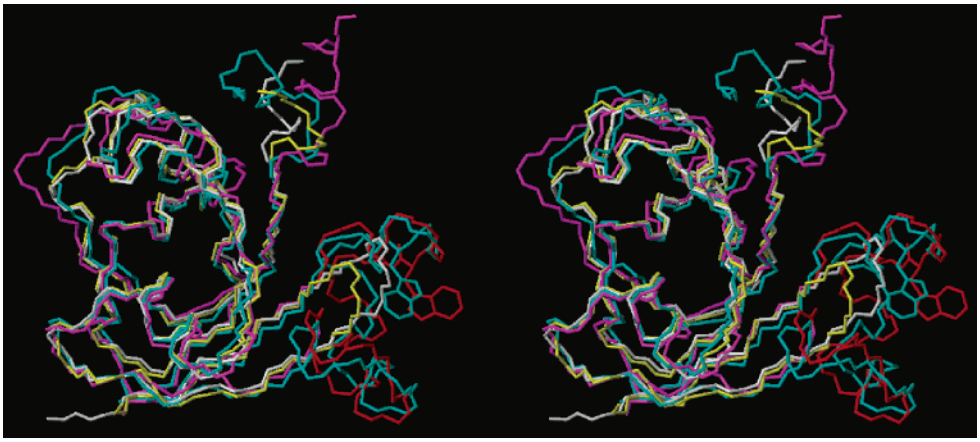

FIGURE 5: Structural comparison of the halophilic ferredoxins from *H. salinarum* (magenta and red) and *Ha. marismortui* (cyan; PDB entry 1DOI) and the plant-type ferredoxins from *Anabaena* 7120 (white; PDB entry 1FXA) and *E. arvense* (yellow; PDB entry 1FRR) in stereoview. The backbone superposition was calculated using DALI (*29*). The extra domain of HsFdx is marked in red, and the side chain of Trp16 is shown for HsFdx and HmFdx.

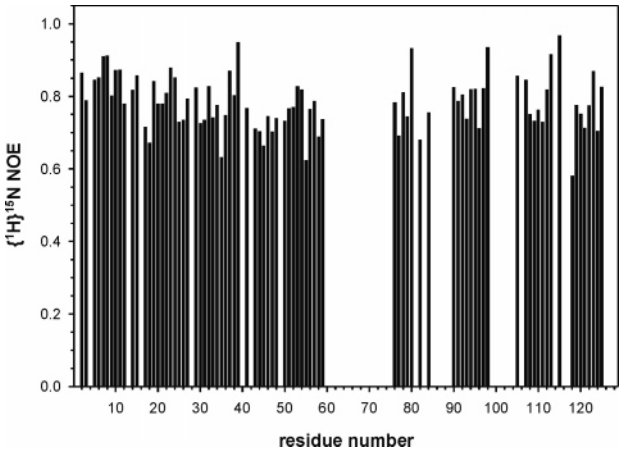

FIGURE 6: $\{^1H\}^{15}N$ NOE of the ^{15}N peak intensities with and without saturation of the amide protons correlated to their sequence position.

in 450 mM NaCl on the picosecond to nanosecond time scale. For most residues, the heteronuclear NOE is larger than 0.65 (Figure 6), indicating a highly restricted internal motion of the NH bond vector, consistent with an overall rigid fold. The observation of $\{^1H\}^{15}N$ NOEs greater than the theoretical maximum (0.82 at 600 MHz) can be attributed to chemical exchange between water and the amide protons (*43*, *53*, *54*).

The extra domain (residues 7−36) and the core fold do not differ with respect to their $\{^1H\}^{15}N$ NOE values, indicating that the local dynamics of both domains is quite similar. Large $\{^1H\}^{15}N$ NOE values are also observed for those peptide stretches (residues 5−9 and 35−39) that connect the core and extra domain, and thus, there is no evidence for the existence of flexible hinges. This finding is consistent with the observation of numerous NOEs between both parts of the molecule.

Protein Denaturation. To accelerate the denaturation process, this experiment was performed at 40 °C instead of 15 °C. There were only moderate shifts of the resonances compared to the spectra acquired at 15 °C, allowing an unambiguous resonance assignment in the $^1H-^{15}N$ HSQC spectrum. Denaturation of HsFdx at 40 °C was monitored by measuring the decrease in signal intensity in a series of HSQC spectra collected over a total of 70 h. Most of the resonances show a uniform decrease in the signal intensity, leading to values of 45−60% of the original intensity after 70 h (data not shown). For a few cross-peaks, no decrease in signal intensity was detected. This can most likely be explained by the fact that the apoprotein which is formed during the denaturation process exhibits the same chemical shifts as the holo form for these residues. Monitoring protein denaturation by NMR thus did not reveal any differences between the core fold and the acidic extra domain, suggesting a cooperative unfolding of both parts of the molecule.

Table 3: Expression Efficiency of HsFdx and Its Mutant Δ-HsFdx in the Halophilic Organism *H. salinarum* and the Mesophilic Organism *E. coli*

protein	expression in *H. salinarum*	protein	expression in *E. coli*
$HsFdx(His)_6$	(+)	HsFdx	−
Δ-$HsFdx(His)_6$	−	Δ-HsFdx	++
BR−HsFdx	++	GST−HsFdx	+
BR−Δ-HsFdx	−	GST−Δ-HsFdx	++

Mutant of the H. salinarum Ferredoxin. NMR spectroscopy has shown that the acidic extra domain does not differ from the remaining parts of the protein with respect to its dynamics or unfolding behavior, making it difficult to draw final conclusions about the role of this region in halophilic adaptation. To allow a rigorous investigation of this point, a mutant of HsFdx (Δ-HsFdx) was designed that lacks the extra domain (α′ and α″).

In Figure 5, an overlay of the backbone Cα traces of HsFdx with *Anabaena* 7120 ferredoxin is depicted. Both structures are very similar; the only big difference is the insertion of the two α-helices, α′ and α″, in HsFdx between strands β_1 and β_2, whereas *Anabaena* ferredoxin contains a loop at this position. For the mutant, the 30 additional amino acids in the halophilic ferredoxin have been replaced with the loop of *Anabaena* ferredoxin.

Expression of HsFdx and Δ-HsFdx. The expression of several constructs of HsFdx on one side and of its mutant Δ-HsFdx on the other side has been tested in *H. salinarum* and *E. coli* (Table 3). The expression efficiency has been judged from the significance of the bands in SDS−PAGE corresponding to HsFdx and Δ-HsFdx. HsFdx was recombinantly expressed in *H. salinarum* in small quantities as a

Table 4: Reconstitution of Apo-HsFdx in Correlation to the Salt Concentration[a]

	1	2	3	4	5
[NaCl] (M)	0.00	0.15	0.43	2.00	4.3
A_{420}/A_{280} after reconstitution	0.00	0.00	0.20	0.33	0.33

[a] Twenty microliters each of 100 mM $FeSO_4$ and 100 mM Na_2S were added to 400 μL of a 125 μM solution of apo-HsFdx. The pH of the solution after reconstitution and dialysis was 7.3.

His-tagged protein and in large amounts as a fusion with bacteriorhodopsin. In *E. coli*, only a low level of expression of the GST−HsFdx fusion protein [fusion with glutathione *S*-transferase (GST)] was obtained, whereas Δ-HsFdx was expressed in large amounts with and without the tag. No expression at all was seen for Δ-HsFdx in *H. salinarum*, demonstrating a clear preference of the halophilic expression host for the halophilic ferredoxin and of the mesophilic organism for the mutated ferredoxin.

Reconstitution and Folding. A reconstitution protocol was established for HsFdx (see also Experimental Procedures). The apo form was prepared from the holoferredoxin by addition of trichloroacetic acid. Addition of $FeSO_4$ (or $FeCl_3$) and Na_2S was followed by dialysis against buffers at neutral pH. The reconstitution efficiency is strongly dependent on the salt concentration of the dialysis buffer. Up to a concentration of 150 mM NaCl, no cluster reconstitution is observed (Table 4). At 430 mM, holo-HsFdx is formed with a lower absorption coefficient than the pure HsFdx. Only at a salt concentration of more than 2.0 M NaCl is the holoprotein with an A_{420}/A_{280} absorption ratio typical for HsFdx with intact tertiary structure formed.

The mutant ferredoxin Δ-HsFdx is expressed as the apoprotein in *E. coli* like many other ferredoxins (*55*, *56*). It has been found that a couple of other proteins are involved in the formation and incorporation of iron−sulfur clusters. The proteins are encoded in the so-called *isc* gene cluster (iron−sulfur cluster) (*57*−*59*). The gene sequences for proteins homologous to NifS and NifU are also present in the genome of *H. salinarum* (www.Halolex.mpg.de). The overexpression of the isc cluster is found to greatly enhance the formation of holo- instead of apoferredoxins. The expression of Δ-HsFdx was performed without overexpression of the isc cluster. Thus, it was not surprising that apo-Δ-HsFdx was obtained, rendering a reconstitution of the iron−sulfur cluster necessary. The reconstitution of the iron−sulfur cluster into Δ-HsFdx was performed in the crude cytosolic fraction of the expression medium (see Reconstitution and Purification of Δ-HsFdx in Experimental Procedures). When Tris buffer containing 2 M NaCl was used in the dilution step, the absorption intensity at 420 nm of the resulting solution was only 20% compared to that of a solution containing reconstituted Δ-HsFdx obtained by employing salt-free Tris buffer. Furthermore, storage of the cytosolic fraction after reconstitution at 4 °C for 2 days resulted in a 15% reduction of the absorption at 420 nm when the NaCl concentration was adjusted to 150 mM, whereas the absorption intensity at 420 nm decreased by 45% in 2 days when the solution contained 1 M NaCl. These results demonstrate that the reconstitution efficiency as well as the stability of the mutant ferredoxin Δ-HsFdx decreases with an increase in salt concentration.

After the reconstitution, Δ-HsFdx was purified in a manner analogous to the purification procedure for *Anabaena* ferredoxin from Jacobson et al. (*60*). During the purification, the absorption of Δ-HsFdx at 420 nm significantly decreases with every purification step, and the CD spectra of the purified mutant show that the protein has no regular secondary structure. Reconstitution of Δ-HsFdx after purification was also assayed but proved not to be successful (*12*). To test whether additional proteins of the cytosolic fraction are required for reconstitution of the iron−sulfur cluster into apo-Δ-HsFdx, *E. coli* cytosol has been added to the purified mutant protein Δ-HsFdx. However, the addition of cytosol to the purified mutant ferredoxin did not support its reconstitution with the iron−sulfur cluster and refolding either. This result can be explained by the fact that the mutant Δ-HsFdx is denatured irreversibly during the purification.

Taken together, the reconstitution experiments described above show that the halophilic ferredoxin HsFdx can only be reconstituted at high salt concentrations. The integration of the iron−sulfur cluster prompts (or triggers) the correct folding of the halophilic ferredoxin. In contrast thereto, the iron−sulfur cluster of the mutant Δ-HsFdx is reconstituted into the protein with higher efficiency at low salt concentrations. Although the iron−sulfur cluster can be incorporated into Δ-HsFdx, no formation of regular secondary structure is observed in the mutant Δ-HsFdx. These results show that the replacement of the negatively charged extra region has a marked influence on the reconstitution behavior of the ferredoxin as it reverses the salt dependence of the iron−sulfur cluster incorporation. Although the two α-helices of HsFdx are positioned opposite from the hydrophobic part around the active center of the Fe_2S_2 cluster, it is possible that the correct conformation of the two α-helices under high-salt conditions is necessary for cluster incorporation. These findings suggest a role for the extra domain in the proper folding of HsFdx at high salt concentrations.

Different Kind of Adaptation? HsFdx exhibits a salt-dependent stability typical for halophilic proteins (Table 1 and Figure 2). The solution structure, which was determined from the NMR data, showed no significant differences from the crystal structure of the homologous halophilic ferredoxin HmFdx. This is striking because the NMR spectra have been acquired at salt concentrations of ∼450 mM NaCl, and the crystals of HmFdx were grown at 4 M sodium phosphate. It was generally believed that high salt concentrations are required to shield the negative charges of the carboxylic residues on the surface of the halophilic protein. However, the agglomeration of negatively charged residues on the surface of HsFdx did not show a destabilizing effect on the secondary structure of the acidic domain at salt concentrations as low as 450 mM NaCl. Furthermore, no increased flexibility of the acidic domain or a stronger tendency to unfold compared to the rest of the protein could be observed, as the analysis of the flexibility and the denaturation kinetics of HsFdx showed that the protein is rigid and that the unfolding of HsFdx is a cooperative process.

Wild-type HsFdx and its mutant Δ-HsFdx show opposed expression efficiencies in *H. salinarum* and *E. coli*. In addition, the replacement of the acidic extra domain leads to a change in the salt dependence of the reconstitution of the iron−sulfur cluster. The integration of the cluster in HsFdx only takes place at high salt concentrations, whereas

low-salt solutions support the reconstitution of the iron−sulfur cluster into the mutant Δ-HsFdx.

We propose that the acidic insertion of 30 amino acids could be a means for rapid adaptation of proteins, which are acquired by lateral gene transfer, to the high salt concentration inside an extremely halophilic organism. This proposal is corroborated by a systematic screen of the genome of *H. salinarum* (V. Hickmann, F. Pfeiffer, and D. Oesterhelt, unpublished results). Stretches of 30 amino acids with more than 50% acidic residues are found ubiquitously on the chromosome and total ∼240 instances. Systematic bioinformatic analysis and structural modeling are being carried out to support our hypothesis. Long-term adaptation by covering the surface, on the other hand, can be shown by homology-based genome-wide structural modeling and has been demonstrated experimentally for a few conspicuous cases (*61*−*63*).

ACKNOWLEDGMENT

We thank Prof. P. Rösch for NMR time at the DRX600 spectrometer in Bayreuth.

REFERENCES

1. Ginzburg, M., Sachs, L., and Ginzburg, B. Z. (1970) Ion metabolism in a *Halobacterium*, *J. Gen. Phys. 55*, 187−206.
2. Eisenberg, H., Mevarech, M., and Zaccai, G. (1992) Biochemical, structural, and molecular genetic aspects of halophilism, *Adv. Protein Chem. 43*, 1−62.
3. Frolow, F., Harel, M., and Sussman, J. L. (1996) Insights into protein adaptation to a saturated salt environment from the crystal structure of a halophilic 2Fe-2S ferredoxin, *Nat. Struct. Biol. 3*, 452−458.
4. Dym, O., Mevarech, M., and Sussmann, J. L. (1995) Structural features that stabilize halophilic malate dehydrogenase from an archaebacterium, *Science 267*, 1344−1346.
5. Hase, T., Wakabayashi, S., Matsubura, H., Kerscher, L., Oesterhelt, D., Rao, K. K., and Hall, D. O. (1977) *Halobacterium halobium* ferredoxin: A homologous protein to chloroplast-type ferredoxins, *FEBS Lett. 77*, 308−310.
6. Kerscher, L., and Oesterhelt, D. (1981) The catalytic mechanism of 2-oxoacid:ferredoxin oxidoreductases from *Halobacterium halobium*, *Eur. J. Biochem. 116*, 595−600.
7. Pfeifer, F., Griffig, J., and Oesterhelt, D. (1993) The fdx gene encoding the [2Fe-2S] ferredoxin of *Halobacterium salinarum* (*H. halobium*), *Mol. Gen. Genet. 239*, 66−71.
8. Wagner, G., Oesterhelt, D., Krippahl, G., and Lanyi, J. K. (1981) Bioenergetic role of halorhodopsin in *Halobacterium salinarum* cells, *FEBS Lett. 131*, 13502−13510.
9. Pfeiffer, M., Rink, T., Gerwert, K., Oesterhelt, D., and Steinhoff, H.-J. (1999) Site-directed spin-labeling reveals the orientation of the amino acid side chains in the E−F loop of bacteriorhodopsin, *J. Mol. Biol. 287*, 163−171.
10. Studier, F. W., and Moffatt, B. A. (1986) Use of bacteriophage-T7 RNA polymerase to direct selective high-level expression of cloned genes, *J. Mol. Biol. 189*, 113−130.
11. Besir, H. (2001) Ph.D. Dissertation, Ludwig-Maximilians-University, Munich, Germany.
12. Marg, B.-L. (2002) Ph.D. Dissertation, Ludwig-Maximilians-University, Munich, Germany.
13. Cline, S. W., Schalkwyk, L. C., and Doolittle, W. F. (1989) Transformation of the archaeabacterium *Halobacterium volcanii* with genomic DNA, *J. Bacteriol. 171*, 4987−4991.
14. Oesterhelt, D. (1995) Isolation of Purple Membranes, in *Archaea, a Laboratory Manual* (DasSarma, S., and Fleischmann, E. M., Eds.) Cold Spring Harbor Laboratory Press, Plainview, NY.
15. Schweimer, K., Marg, B.-L., Oesterhelt, D., Rosch, P., and Sticht, H. (2000) Sequence-specific ^{1}H, ^{13}C and ^{15}N resonance assignments and secondary structure of [2Fe-2S] ferredoxin from *Halobacterium salinarum*, *J. Biomol. NMR 16*, 347−348.
16. Talluri, S., and Wagner, G. (1996) An Optimized 3D NOESY-HSQC, *J. Magn. Reson. 112*, 200−205.
17. Cavanagh, J., Fairbrother, W. J., Palmer, A. G., and Skelton, N. J. (1996) *Protein NMR Spectroscopy*, Academic Press, San Diego, CA.
18. Ikura, M., Bax, A., Clore, G. M., and Gronenborn, A. M. (1990) Detection of nuclear Overhauser effects between degenerate amide proton resonances by heteronuclear 3D NMR spectroscopy, *J. Am. Chem. Soc. 112*, 9020−9022.
19. Sklenar, V., Piotto, M., Leppik, R., and Saudek, V. (1993) Gradient-tailored water suppression for ^{1}H-^{15}N HSQC experiments optimized to retain full sensitivity, *J. Magn. Reson. 102A*, 241−245.
20. Schleucher, J., Schwendinger, M., Sattler, M., Schmidt, P., Schedletzky, O., Glaser, S. J., Sørensen, O. W., and Griesinger, C. (1994) A general enhancement scheme in heteronuclear multidimensional NMR employing pulsed field gradients, *J. Biomol. NMR 4*, 301−306.
21. Marion, D., Ikura, M., Tschudin, R., and Bax, A. (1989) Rapid recording of 2D NMR spectra without phase cycling. Applications to the study of hydrogen exchange in proteins, *J. Magn. Reson. 85*, 393−399.
22. Dayie, K. T., and Wagner, G. (1994) Relaxation-rate measurements for ^{15}N-^{1}H groups with pulsed field gradients and preservation of coherence pathways, *J. Magn. Reson. 111A*, 121−126.
23. Johnson, B. A., and Blevins, R. A. (1994) NMRView: A computer program for the visualization and analysis of NMR data, *J. Biomol. NMR 4*, 603−614.
24. Brünger, A. T. (1993) *X-PLOR*, version 3.1, Howard Hughes Medical Institute and Yale University, New Haven, CT.
25. Nilges, M., and O'Donoghue, S. I. (1998) Ambiguous NOEs and automated NOE assignment, *Prog. NMR Spectrosc. 32*, 107−139.
26. Folmer, R. H., Hilbers, C. W., Konings, R. N., and Nilges, M. (1997) Floating stereospecific assignment revisited: Application to an 18 kDa protein and comparison with J-coupling data, *J. Biomol. NMR 9*, 245−258.
27. Kabsch, W., and Sander, C. (1983) Dictionary of protein secondary structure: Pattern recognition of hydrogen-bonded and geometrical features, *Biopolymers 22*, 2577−2637.
28. Laskowski, R. A., MacArthur, M. W., Moss, D. S., and Thornton, J. M. (1993) PROCHECK: A program to check the stereochemical quality of protein structures, *J. Appl. Crystallogr. 26*, 283−291.
29. Holm, L., and Sander, C. (1996) Mapping the protein universe, *Science 273*, 595−603.
30. Nicholls, A. (1993) *GRASP: Graphical representation and analysis of surface properties*, Columbia University, New York.
31. Kraulis, P. (1991) MOLSCRIPT: A program to produce both detailed and schematic plots of protein structures, *J. Appl. Crystallogr. 24*, 946−950.
32. Merritt, E. A., and Murphy, M. E. P. (1994) Raster3D version 2.0: A programme for photorealistic molecular graphics, *Acta Crystallogr. D50*, 869−873.
33. Oesterhelt, D., and Kerscher, L. (1995) Isolation of Halophilic Archaeal Ferredoxin, in *Archaea, a laboratory manual. Halophiles* (DasSarma, S., and Fleischmann, E. M., Eds.) Cold Spring Harbor Laboratory Press, Plainview, NY.
34. Werber, M. M., and Mevarech, M. (1978) Purification and characterization of a highly acidic 2Fe−Ferredoxin from *Halobacterium* of the Dead Sea, *Arch. Biochem. Biophys. 187*, 447−456.
35. Bandyopadhyay, A. K., and Sonawat, H. M. (2000) Salt dependent stability and unfolding of [Fe2−S2] ferredoxin of *Halobacterium salinarum*: Spectroscopic investigations, *Biophys. J. 79*, 501−510.
36. Mevarech, M., Frolow, F., and Gloss, L. M. (2000) Halophilic enzymes: Proteins with a grain of salt, *Biophys. Chem. 86*, 155−164.
37. Bandyopadhyay, A. K., Krishnamoorthy, G., and Sonawat, H. M. (2001) Structural stabilization of [2Fe-2S] ferredoxin from *Halobacterium salinarum*, *Biochemistry 40*, 1284−1292.
38. Oh, B. H., and Markley, J. L. (1990) Multinuclear magnetic resonance studies of the 2Fe.2S* ferredoxin from *Anabaena* species strain PCC 7120. 1. Sequence-specific hydrogen-1 resonance assignments and secondary structure in solution of the oxidized form, *Biochemistry 29*, 3993−4004.
39. Im, S. C., Liu, G., Luchinat, C., Sykes, A. G., and Bertini, I. (1998) The solution structure of parsley [2Fe-2S]ferredoxin, *Eur. J. Biochem. 258*, 465−477.
40. Pochapsky, T. C., Ye, X. M., Ratnaswamy, G., and Lyon, T. A. (1994) An NMR-derived model for the solution structure of

oxidized putidaredoxin, a 2-Fe, 2-S ferredoxin from *Pseudomonas*, *Biochemistry 33*, 6424−6432.
41. Lelong, C., Setif, P., Bottin, H., Andre, F., and Neumann, J. M. (1995) ^{1}H and ^{15}N NMR sequential assignment, secondary structure, and tertiary fold of [2Fe-2S] ferredoxin from *Synechocystis* sp. PCC 6803, *Biochemistry 34*, 14462−14473.
42. Goodfellow, B. J., and Macedo, A. L. (1999) NMR structural studies of iron−sulfur proteins, *Annu. Rev. NMR Spectrosc. 37*, 119−177.
43. Kazanis, S., and Pochapsky, T. C. (1997) Structural features of the metal binding site and dynamics of gallium putidaredoxin, a diamagnetic derivative of a Cys4Fe2S2 ferredoxin, *J. Biomol. NMR 9*, 337−346.
44. Vo, E., Wang, H. C., and Germanas, J. P. (1997) Preparation and characterization of [2Ga-2S] *Anabaena* 7120 ferredoxin, the first gallium−sulfur cluster-containing protein, *J. Am. Chem. Soc. 119*, 1934−1940.
45. Johnson, K. A., Brereton, P. S., Verhagen, M. F., Calzolai, L., La Mar, G. N., Adams, M. W., and Amster, I. J. (2001) A gallium-substituted cubane-type cluster in *Pyrococcus furiosus* ferredoxin, *J. Am. Chem. Soc. 123*, 7935−7936.
46. Donaire, A., Zhou, Z. H., Adams, M. M., and La Mar, G. N. (1996) ^{1}H NMR investigation of the secondary structure, tertiary contacts and cluster environment of the four-iron ferredoxin from the hyperthermophilic archaeon *Thermococcus litoralis*, *J. Biomol. NMR 7*, 35−47.
47. Bertini, I., Turano, P., and Vila, A. J. (1993) Nuclear magnetic resonance of paramagnetic metalloproteins, *Chem. Rev. 93*, 2833−2932.
48. Sticht, H., and Rösch, P. (1998) The structure of iron−sulfur proteins, *Prog. Biophys. Mol. Biol. 70*, 95−136.
49. Rypniewski, W. R., Breiter, D. R., Benning, M. M., Wesenberg, G., Oh, B. H., Markley, J. L., Rayment, I., and Holden, H. M. (1991) Crystallization and structure determination to 2.5 Å resolution of the oxidized [2Fe-2S] ferredoxin isolated from *Anabaena* 7120, *Biochemistry 30*, 4126−4131.
50. Ikemizu, S., Bando, M., Sato, T., Morimoto, Y., and Tsukihara, T. (1994) Structure of the [2Fe-2S]-ferredoxin I from *Equisetum arvense* at 1.8 Å resolution, *Acta Crystallogr. D50*, 167−174.
51. Zaccai, G., Cendrin, F., Haik, Y., Borochov, N., and Eisenberg, H. (1989) Stabilization of halophilic malate dehydrogenase, *J. Mol. Biol. 208*, 491−500.
52. Richard, S. B., Madern, D., Garcin, E., and Zaccai, G. (2000) Halophilic adaptation: Novel solvent protein interactions observed in the 2.9 and 2.6 Å resolution structures of the wild type and a mutant of malate dehydrogenase from *Haloarcula marismortui*, *Biochemistry 39*, 992−1000.
53. Clore, G. M., Driscoll, P. C., Wingfield, P. T., and Gronenborn, A. M. (1990) Analysis of the backbone dynamics of interleukin-1β using two-dimensional inverse detected heteronuclear ^{15}N-^{1}H NMR spectroscopy, *Biochemistry 29*, 7387−7401.
54. Powers, R., Clore, G. M., Stahl, S. J., Wingfield, P. T., and Gronenborn, A. (1992) Analysis of the backbone dynamics of the ribonuclease H domain of the human immunodeficiency virus reverse transcriptase using ^{15}N relaxation measurements, *Biochemistry 31*, 9150−9157.
55. Cheng, H., Westler, W. M., Xia, B., Oh, B.-H., and Markley, J. L. (1995) Protein Expression, Selective Isotopic Labeling, and Analysis of Hyperfine-Shifted NMR Signals of *Anabaena* 7120 Vegetative [2Fe-2S] Ferredoxin, *Arch. Biochem. Biophys. 316*, 619−634.
56. Xia, B., Cheng, H., Bandarian, V., Reed, G. H., and Markley, J. L. (1996) Human ferredoxin: Overproduction in *Escherichia coli*, reconstitution in vitro, and spectroscopic studies of iron−sulfur cluster ligand cysteine-to serine mutants, *Biochemistry 35*, 9488−9495.
57. Nakamura, M., Saeki, K., and Takahashi, Y. (1999) Hyperproduction of recombinant ferredoxins in *Escherichia coli* by coexpression of the ORF1-ORF2-iscS-iscU-iscA-hscB-hscA-fdx-ORF3 gene cluster, *J. Biochem. 126*, 10−18.
58. Zheng, L., Cash, V. L., Flint, D. H., and Dean, D. R. (1998) Assembly of iron−sulfur clusters, *J. Biol. Chem. 273*, 13264−13272.
59. Agar, J. N., Krebs, C., Frazzon, J., Huynh, B. H., Dean, D. R. J., and Johnson, M. K. (2000) IscU as a scaffold for iron−sulfur cluster biosynthesis: Sequential assembly of [2Fe-2S] and [4Fe-4S] clusters in IscU, *Biochemistry 39*, 7856−7862.
60. Jacobson, B. L., Chae, Y. K., Böhme, H., Markley, J. L., and Holden, H. M. (1992) Crystallization and preliminary analysis of oxidized, recombinant, heterocyst [2Fe-2S] ferrecodoxin from *Anabaena* 7120, *Arch. Biochem. Biophys. 294*, 279−281.
61. Ebel, Ch., Cosenaro, L., Pascu, M., Faou, P., Kernel, B., Proust-De martin, F., and Zaccai, J. (2002) Solvent interaction of halophilic malate dehydrogenase, *Biochemistry 41*, 13234−13252.
62. Bieger, B., Essen, L.-O., and Oesterhelt, D. (2003) Crystal structure of halophilic dodecin: A novel, dodecameric flavin binding protein from *Halobacterium salinarum*, *Structure 11*, 375−385.
63. Zeth, K., Offermann, S., Essen, L.-O., and Oesterhelt, D. (2004) Iron-oxo clusters biomineralizing on protein surfaces? Structural analysis of *H. salinarum* DpsA in its low and high iron states, *Proc. Natl. Acad. Sci. U.S.A.* (in press).
64. Higgins, D. G., Bleasby, A. J., and Fuchs, R. (1992) CLUSTAL V: Improved software for multiple sequence alignment, *Comput. Appl. Biosci. 8*, 189−191.
65. Barton, G. J. (1993) ALSCRIPT: A tool to format multiple sequence alignments, *Protein Eng. 6*, 37−40.

BI0485169